University of Massachusetts Amherst

ScholarWorks@UMass Amherst

Masters Theses   Dissertations and Theses

November 2015

Studying Nanoparticle/cell and Nanoparticle/biosurface Interaction with Mass Spectrometry

Singyuk Hou
University of Massachusetts Amherst

Follow this and additional works at: https://scholarworks.umass.edu/masters_theses_2

Part of the Analytical Chemistry Commons, Biotechnology Commons, and the Materials Chemistry Commons

STUDYING NANOPARTICLE/CELL AND NANOPARTICLE/BIOSURFACE INTERACTION WITH MASS SPECTROMETRY

A Thesis Presented

by

SINGYUK HOU

Submitted to Graduate School of the

University of Massachusetts Amherst in partial fulfillment

of the requirements for the degree of

MASTER OF SCIENCE

September 2015

Chemistry

STUDYING NANOPARTICLE/CELL AND NANOPARTICLE/BIOSURFACE INTERACTION WITH MASS SPECTROMETRY

A Thesis Presented

by

SINGYUK HOU

Approved as to style and content by:

_____

Vincent M. Rotello, Co-chair

_____

Richard W. Vachet, Co-chair

_____

Craig T. Martin, Department Head

Department of Chemistry

ACKNOWLEDGEMENTS

ABSTRACT

STUDYING NANOPARTICLE/CELL AND NANOPARTICLE/BIOSURFACE INTERACTION WITH MASS SPECTROMETRY

SEPTEMBER 2015

SINGYUK HOU

B.S., WUHAN UNIVERSITY

M.S., UNIVERSITY OF MASSACHUSETTS AMHERST

Directed by: Professor Richard W. Vachet and Professor Vincent M. Rotello

Nanoparticles (NPs) have been used widely in various fields ranging from biomedical applications to life science due to their highly tunable properties. It is essential to understanding how NPs interact with biological systems of interest, therefore, analytical platforms to efficiently track NPs from cell to animal level are essential. In this thesis, laser desorption ionization mass spectrometry (LDI-MS) and inductively-coupled plasma mass spectrometry (ICP-MS) has been developed and applied to quantify NP/cell and NP/biological surface interactions. These two methods provide fast, label-free and quantitative analysis. New capability of LDI-MS to differentiate cell surface-bound and internalized NPs were established and ICP-MS coupled with a library of surface-functionalized AuNPs were used to probe the affinity between NPs and human hair surface. NPs interacting with biological surfaces and plasma membrane were quantified and the interactions were controlled by the chemical properties of the interface between NP and biological systems.

TABLE OF CONTENTS

LIST OF FIGURES

CHAPTER 1

DIFFERENTIATION BETWEEN CELL SURFACE-BOUND AND INTERNALIZED NANOPARTICLES USING LASER DESOPRTION/IONIZAITON MASS SPECTROMETRY

1.1 Introduction

The ability to finely control the size,[1] shape[2] and surface properties[3] of nanoparticles (NPs) coupled with their ability to provide controlled release[4,5] makes them potent carriers for cellular delivery of therapeutics. The unique optical and magnetic properties of NP cores likewise make them important imaging reagents.[6,7] The localization of these materials is, however, essential to their utility with efficiency of cellular uptake is a key figure of merit in the engineering of NPs for biomedical applications. Most strategies for achieving uptake, however, rely on modification of NPs with ligands designed to interact with specific receptors or to interact strongly with the plasma membrane.[8,9] Both strategies will generate simultaneous cell surface adhesion and internalization, with very different therapeutic/imaging outcomes for these two locations.

Despite the central importance of quantifying cellular uptake, quantitative differentiation of internalized and cell surface-bound NPs remains a significant challenge.[10] Confocal optical microscopy[11] and transmission electron microscopy (TEM)[12] enable the visualization of cell surface-bound versus internalized NPs. Issues such as aggregation[13] and self-quenching[14] make quantification challenging using optical microscopy, and TEM is not suitable for high-throughput strategies.

In practice, quantitation of the NP cell uptake typically uses either inductively-coupled plasma mass spectrometry (ICP-MS) or flow cytometry.[15,16] Despite the sensitivity and generality of these methods, they do not differentiate cell surface bound and internalized NPs. Chemical etching of extracellular NPs has been used as a strategy to look separately at internalized NPs.[17,18] These methods, however, use disruptive conditions including toxic reagents and disruptively low ionic strength[Error! Bookmark not defined.] that limit their applicability.[19]

In this chapter, I present a method that uses tuned laser energy in laser desorption/ionization mass spectrometry (LDI-MS) to rapidly quantify cell surface-bound and internalized NPs. This LDI-MS method quantitatively distinguishes between cell surface-bound and internalized gold nanoparticles (AuNPs) through laser energy absorption by the NP core that then enables desorption and ionization of attached monolayers. [20] LDI-MS is a versatile strategy that has been successfully used to characterize a wide range of NP surface monolayers on a variety of materials.[21,22] This method has also been used to determine cellular uptake[23] and monitor stability of NPs in cells. [24, 25] With these approaches, however, the challenge remained of differentiating internalized and surface-bound particles. In our current study, we show that the proper choice of laser energy allows the selective ionization, detection, and quantitation of NPs on cell surfaces. Combining this method with overall NP amounts then enables the quantitative differentiation of extra- and intracellular NP distributions (Figure 1). We demonstrate the utility of this method through quantitative assessment of the role of proteoglycans in determining cellular uptake of NPs, a challenging question that requires effective differentiation of surface-bound and internalized NPs.
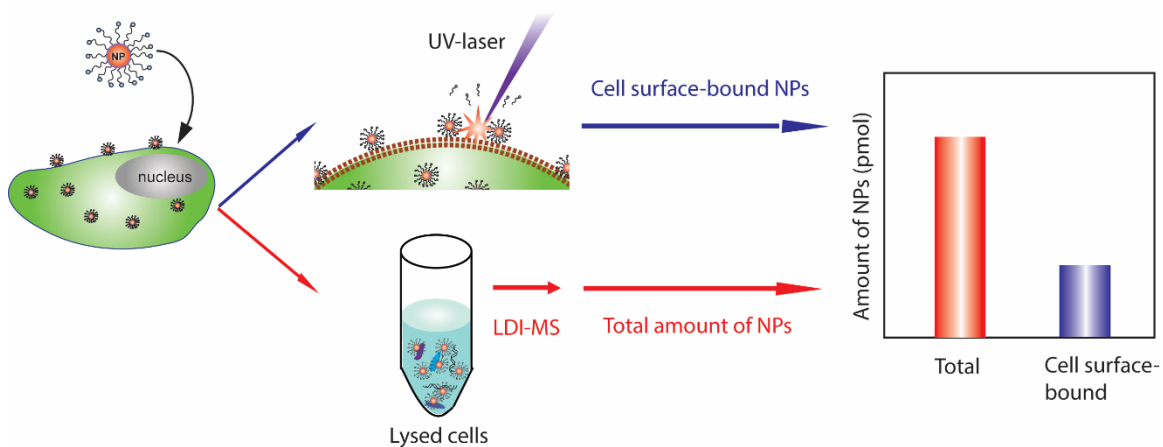
Figure 1.1 Scheme for differentiation between cell surface-bound and internalized NPs with LDI-MS.

1.2 Result and discussion

The hypothesis underlying our research is the laser energy could be tuned to desorb and ionize monolayers from NPs attached to the outside of intact cells but unable to penetrate intact cells membrane to desorb and ionize monolayers from NPs inside the cells. We first determined if AuNPs could be detected on intact cells by studying two cationic AuNPs (Figure 2a). Cells were cultured on indium-tin oxide (ITO) coated glass slide, so that LDI-MS analyses could be performed directly following incubation without further manipulation of the cells. HeLa cells (20,000 cells) were incubated with 250 nM of AuNP 1 and AuNP 2 in serum-free media for 15 min. After incubation, the cells were washed and analyzed by LDI-MS. The mass barcodes of AuNPs 1 and 2 (m/z 464 and 422, respectively) are readily observed in the mass spectrum, as are fragment ions (loss of H_2S from the ligands) and Au^{2+} (m/z 394) ions (Figure 2b).
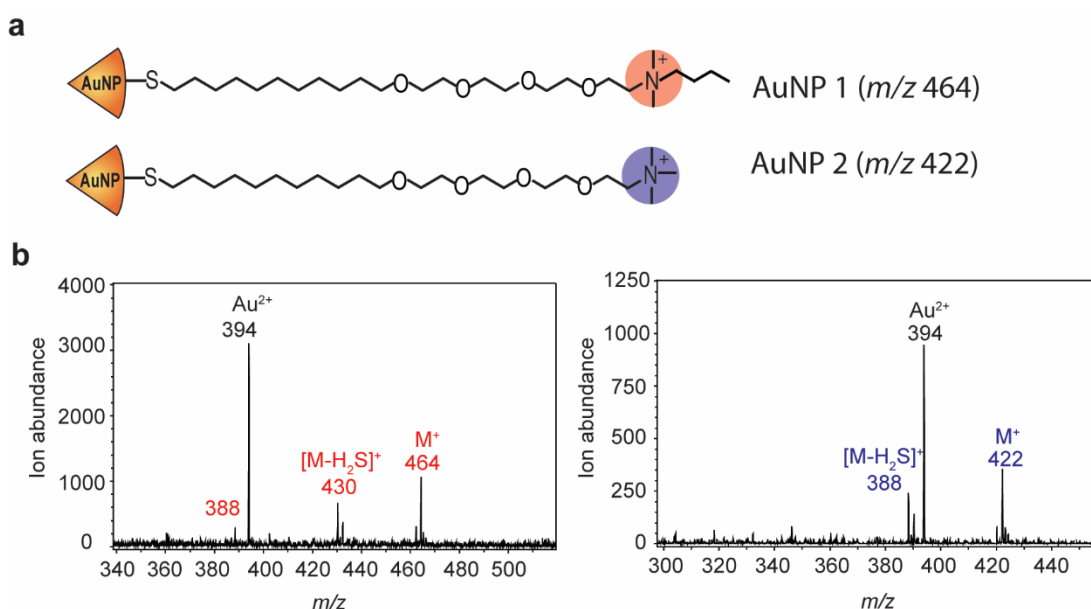
Figure 1.2 Detection of AuNPs present on intact cells. (a) Structures of the monolayer-stabilized AuNPs used in this study and the m/z ratios of their molecular peaks. (b) Mass spectra of AuNP 1 (left) and AuNP 2 (right) detected from a monolayer of intact cells.

We determined the appropriate laser energy for selectively detecting surface-bound AuNPs by sequentially incubating AuNPs 1 and 2 with the cell and analyzing the cell samples by LDI-MS. First, 250 nM of AuNP 1 was incubated with HeLa cells in serum

free media for 60 min. After incubation, the cells were extensively washed with PBS to remove any AuNP 1 that was still bound to the cell surface. From separate ICP-MS measurements, we found that four or more wash cycles were sufficient to remove any AuNPs bound to the cell surface (Figure 3a), leaving only the AuNPs inside the cells. After removal of cell-surface bound AuNP 1, 250 nM of AuNP 2 was then incubated with the cells for different amounts of time to allow AuNP 2 to both bind to the cell surface and be taken up by the cells. As expected, a greater amount of AuNP 2 is associated with the cells after longer incubation times, as measured by LDI-MS of the cell lysate (Figure 3b), indicating that both cell uptake and cell adherence has occurred. During this time the level of AuNP 1 remained unchanged due to the relatively slow rate of exocytosis (Figure 3b).[26] We incubated cells with AuNP 1 for 60 min, followed by washing and incubation with AuNP 2, at time points that provided approximately equal total quantities of the two NPs (Figure 3b). The cells were then subjected to laser irradiation at different energies, and mass spectra were acquired. The signal-to-noise ratios of the mass barcodes for each NP were then compared (Figure 3c). Results show that no ion signal is measured for either AuNP at energies below 38 µJ, but as the laser energy is increased to 38.6 µJ, AuNP 2 is selectively and reproducibly detected. In control experiments using washed and unwashed cells that were incubated with only a single NP, only the unwashed cells provided an ion signal at laser energies below 39 µJ (Figure 6 in Supplementary figures). As the laser energy is further increased past 39 µJ, both AuNPs can be detected from the intact cells, indicating that higher laser energies are sufficient to desorb and ionize NPs both inside and outside the cell. As expected, the NPs outside the cells are detected more efficiently at all the laser energies studied, despite the fact that both NPs are present at approximately equal levels and both NPs have similar ionization efficiencies (Figure 7 in the Supplementary figures). This latter observation is consistent with our initial hypothesis that the cell membrane of intact cells would hinder the desorption/ionization process.
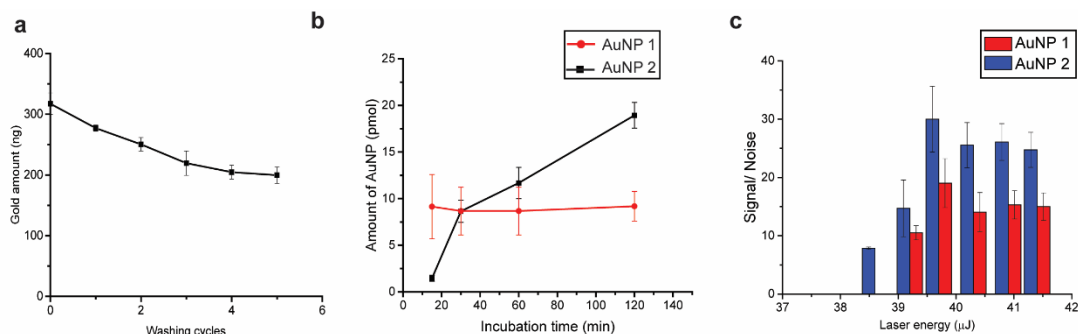
Figure 1.3 Differentiation of cell surface-bound and internalized AuNPs. (a) Workflow for selective detection of AuNPs adsorbed on the plasma membrane by choosing the appropriate laser energy. (b) ICP-MS measurement of AuNP levels in the cell monolayers after increasing numbers of wash cycles. (c) LDI-MS quantification of two AuNPs in cell lysate at different time points of AuNP 2 incubation. Note that AuNP 1 was first incubated for 60 min and then the cell monolayer was washed five times before incubation with AuNP 2. (d) LDI-MS detection of AuNPs 1 and 2 from the intact cell monolayer.
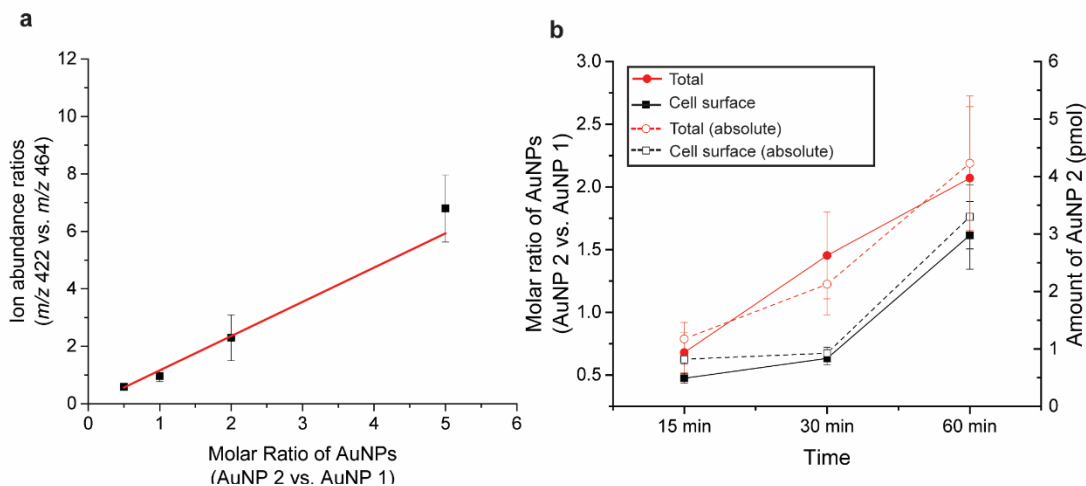
Figure 1.4 Quantification of cell surface-bound and total AuNPs in HepG2 cells. (a) Calibration curve obtained for AuNP 2 (m/z 422) when using AuNP 1 (m/z 464) as the internal standard (b) Relative amounts (solid) and absolute amount (pmol) (dashed) of AuNPs absorbed on cell surface and associated with the entire cells. The absolute amount of total amount of AuNP 2 were measured by ICP-MS and the absolute amount of cell surface AuNP 2 was estimated by using relative quantification shown in the same graph.

5

We next quantified the cell surface-bound AuNPs using an AuNP internal standard and an external calibration. AuNP 1 was used as internal standard; increasing concentrations of AuNP 2 and a fixed concentration of AuNP 1 (100 nM) were incubated with cells for 15 min, during which time minimal NPs were taken up (See Figure 3b). After incubation, the intact cells were immediately analyzed by LDI-MS at the laser energy (i.e. 38.6 μJ) that ionized only cell-surface bound AuNPs. The resulting ion abundance ratios of the mass barcodes for AuNP 2 (m/z 422) and AuNP 1 (m/z 464) were plotted against the concentration ratio between the two AuNPs to generate a calibration curve (Figure 4a). Using this calibration curve, the relative amounts of AuNP 2 bound to the surface of the cells monolayer could be determined (black data points in Figure 4b). For each incubation time indicated, the internal standard (AuNP 1) was added at 100 nM (12.5 pmol) to the incubated sample and allowed to sit with the cells for 15 minutes before LDI-MS analysis. For comparison, a fraction of the cells was also lysed after different incubation times and the total NP content in the cells was determined by LDI-MS (red data points in Figure 4b). The difference between the total (red data) and cell surface bound (black data) amounts allows determination of AuNP 2 uptake (Figure 4b).

We next investigated how different cell-surface proteoglycans influence AuNP internalization as a demonstration of the utility of our method. Wild-type Chinese hamster ovary (CHO) cells and two proteoglycan knockdown mutants, CHO-2 (xylosyltransferase 1 deficient) and CHO-3 (galactosyltransferase 1 deficient) cells were incubated with AuNP 2 and analyzed (Figure 5a) (See Figure 8 in Supplementary figures for calibration curve for these cell lines). No measurable cell uptake occurs during the first 15 minutes of incubation, providing a quantitative measure of NP distributions in these cells using ICP-MS measurements on the cells at the 15 min time point and using these values to correlate ion abundance ratios in Figure 5a and the absolute NP quantity (see Supplementary Information for details). The data in Figure 5b summarize the quantitative NP distributions in the three different cell types. Two observations can be obtained from these data: 1) The NP amounts on the cell surface do not change significantly during the course of incubation, indicating there is a rapidly achieved equilibrium between cell culture media and plasma membrane. 2) The NP amounts bound to plasma membrane differ based on cell glycosylation. The normal CHO cells have a higher level of cell surface adsorption than

the proteoglycan knockdown mutants, consistent with the study by Payne et al. that proposed the importance of negatively charged proteoglycans as binding sites for cationic nanomaterials.[27]
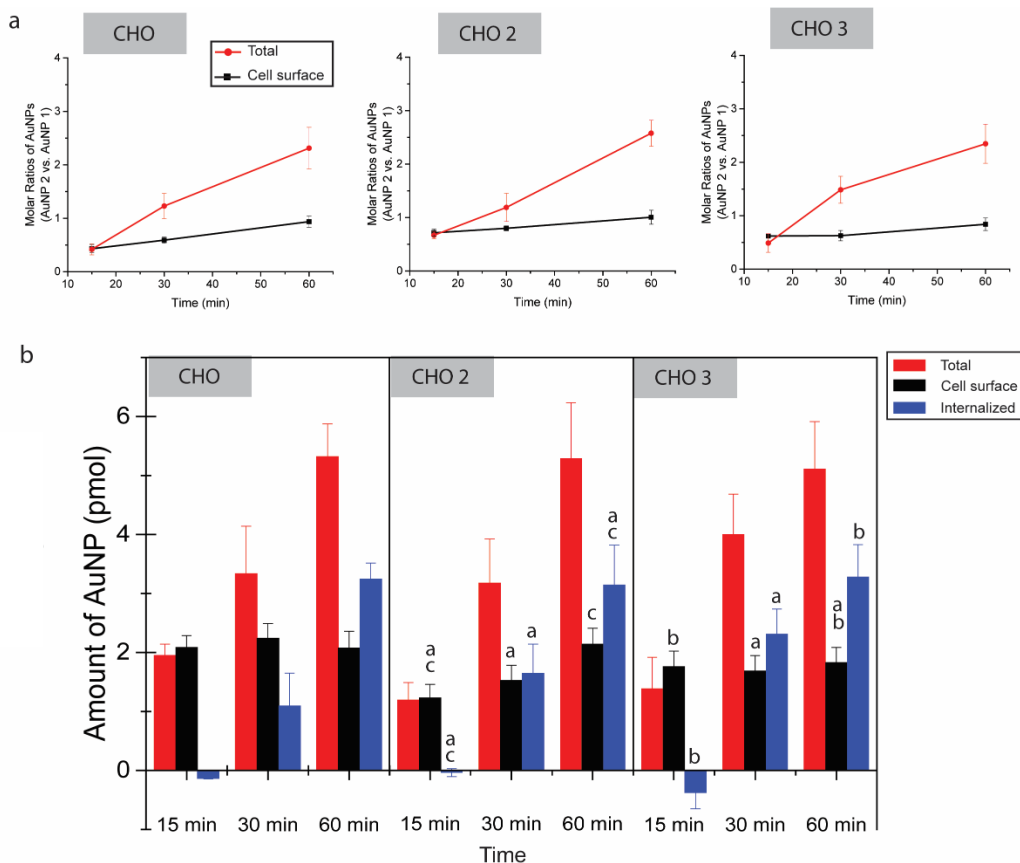
Figure 1.5 Quantities of AuNPs associated with the different CHO cell lines. (a) LDI-MS measurements of cell surface-bound AuNPs and total AuNPs associated with the different CHO cell lines. (b) Absolute quantification of AuNPs associated with the cells after correction with the ICP-MS measurements. One-way-ANOVA (P <0.01) was performed, n= 3, all error bars represent standard deviation. Letters above the bars indicate significance, in which a, b and c are in comparison with CHO, CHO 2 and CHO 3 at the same time point respectively.

1.3 Conclusion

We have shown that cell surface-bound AuNPs can be selectively detected and quantified using LDI-MS by choosing the appropriate laser energy for analysis. Combination of this method with overall NP levels obtained through ICP-MS or LDI-MS

of the cell lysate provides quantitative values for cell surface-bound and internalized NP. This method is rapid, reproducible, and avoids processing conditions that complicate etching-based methods. Given the wide range of nanomaterials that have been shown to be LDI-active,[28, 29, 30, 31] this method provides a highly versatile approach to addressing the long-standing challenge of quantifying nanoparticle internalization.

1.4 Experimental section

Gold nanoparticle synthesis. The gold nanoparticle and ligands were synthesized according to the previous reports.[32] The Brust-Schiffrin two-phase synthesis method was used to synthesize 2 nm core AuNPs.[33] After that, the Murray place-exchange was used to functionalize AuNPs.[34]

Cell culture and interaction with gold nanoparticles. HeLa and HepG2 cells were cultured in a humidified atmosphere (5% CO2) at 37°C and grown in Dulbecco's modified eagle's medium (DMEM, low glucose) supplemented with 10% fetal bovine serum (FBS) and 1% antibiotics (100 U/ml penicillin and 100 μg/ml streptomycin. CHO (ATCC CCL-61), CHO 2 (pgsB-618 (ATCC CRL-2241)) and CHO 3 (pgsA-745 (ATCC CRL-2242)) cells (20,000 cells/well) were cultured in a humidified atmosphere (5% CO_2) at 37°C and grown in F-12K medium supplemented with 10% fetal bovine serum (FBS), 1% antibiotics (100 U/ml penicillin and 100 μg/ml streptomycin) and 1% non-essential amino acids. The cells were split into two groups, one was plated on ITO glass slide and the other was on 96-well plate. After 24 h of plating, the cells were washed three times with cold phosphate buffer saline (PBS). Then, 125 μl of serum free DMEM containing AuNPs was added to the cells at 37°C. After incubation, the cells were washed by cold PBS with one group analyzed directly on ITO glass slide and the other group was lysed for 30 min using lysis buffer (125 μl; Genlantis).

LDI-MS detection and quantification of gold nanoparticles in cell monolayer. ITO glass slides was coated with 0.1% poly-lysine solution for 5 minutes and then washed with deionized water for 3 times to remove excess poly-lysine. The coated slides were then dried in air blow. Open ended Eppendorf (I.D. = 10 mm) tubes were glued to the coated slide on one end to generate media reservoir for cell culture. Planted cells on the slides were used for incubation with AuNPs. After incubation, the reservoirs were removed and

cell monolayer on the substrate were analyzed by LDI-MS. All LDI-MS measurements were carried on a Bruker Autoflex III MALDI-TOF mass spectrometer. All mass spectra were acquired in the reflectron mode with an average of 100 laser shots at a repetition frequency at 100 Hz. The accelerating voltage was set to 19 kV. Bruker software (FlexAnalysis Version 3.3) was used for data analysis. 30 spectrum were collected and averaged for each sample point.

LDI-MS detection and quantification of gold nanoparticles in cell lysate. The lysed cells contained AuNP 1 and/or AuNP 2 were centrifuged at 14,000 r.p.m. for 30 min, cell pellets generated by this process was collected and washed with 60% acetonitrile/40% water to remove excess surfactants. Then, the pellets were transferred onto 384 MTP grounded steel MALDI target for LDI-MS analysis. External calibration curves were generated before sample analyses (See Figure 9 in Supplementary figures). A series amount of AuNP 1 (0, 1, 2, 5, 10 and 20 pmol) and constant amount of AuNP 2 (5 pmol) was spiked into cell lysate and vortexed for 15 min. The resulting pellets from centrifugation were washed and analysed by LDI-MS. The intensity ratios of the molecular ions for both AuNPs were plotted against AuNP molar ratios to generate a calibration curve. The quantity of AuNP were then determined by comparing with the calibration curve.

ICP-MS sample preparation and measurement. After interaction, the lysed cells were digested with 0.5 ml of fresh aqua regia (highly corrosive, use with high caution) for 15 min. The digested samples were diluted to 10 ml with deionized water. A series of gold standard solutions (0, 0.2, 0.5, 1, 2, 5, 10 and 20 ppb) were prepared before each experiment in 5 % aqua regia. The gold standard solutions and cell lysate samples were measured on a Nexion ICP mass spectrometer (PerkinElmer). The instrument was operated with 1,100W radiofrequency power, and the nebulizer argon flow rate was optimized around 0.9 to 1.1 l/ min.

1.5 Supplementary Information
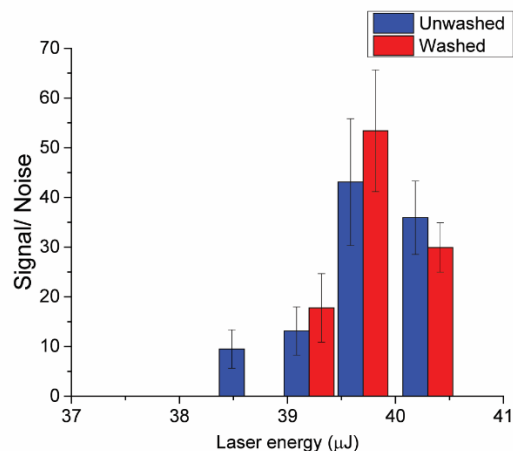
Figure 1.6 LDI-MS of AuNP 2 on cell monolayers before and after washing. 250 nM AuNP 2 was incubated with the cell monolayer for 60 minutes in serum free media at 37 ºC. After incubation, the cell monolayer was either washed four times (washed) or one time (unwashed) before LDI-MS analysis.
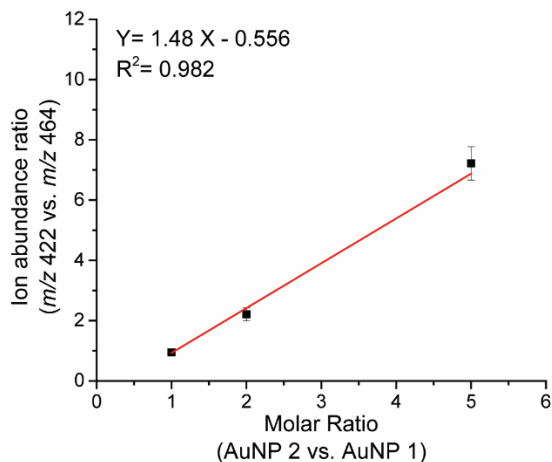
Figure 1.7 Relative ionization efficiency between AuNP 1 and AuNP 2. A constant concentration of AuNP 1 was mixed with different concentrations of AuNP 2 and then analyzed by LDI-MS. The LDI-MS intensity ratios between AuNP 1 and AuNP 2 were then plotted against the molar ratio between the two nanoparticles. The resulting slope from the plot provide information about the relative ionization efficiency of the two AuNPs. A slope closer to 1 indicates that the two AuNPs have more similar ionization efficiencies.
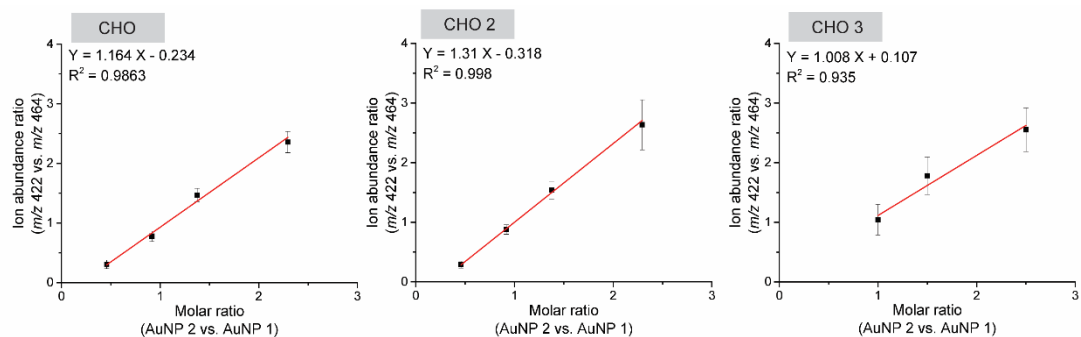
Figure 1.8 LDI-MS calibration curves for AuNP 2 on the cell surface. CHO, CHO 2 and CHO 3 cells were cultured on ITO-glass slide. Increasing concentrations of AuNP 2 were mixed with AuNP 1 (internal standard) and incubated with cells as described in the text. Cells on the glass slide were detected using 38.6 µJ to only detect AuNPs on cell surface. Molecular ions of both AuNPs were plotted against molar ratios.
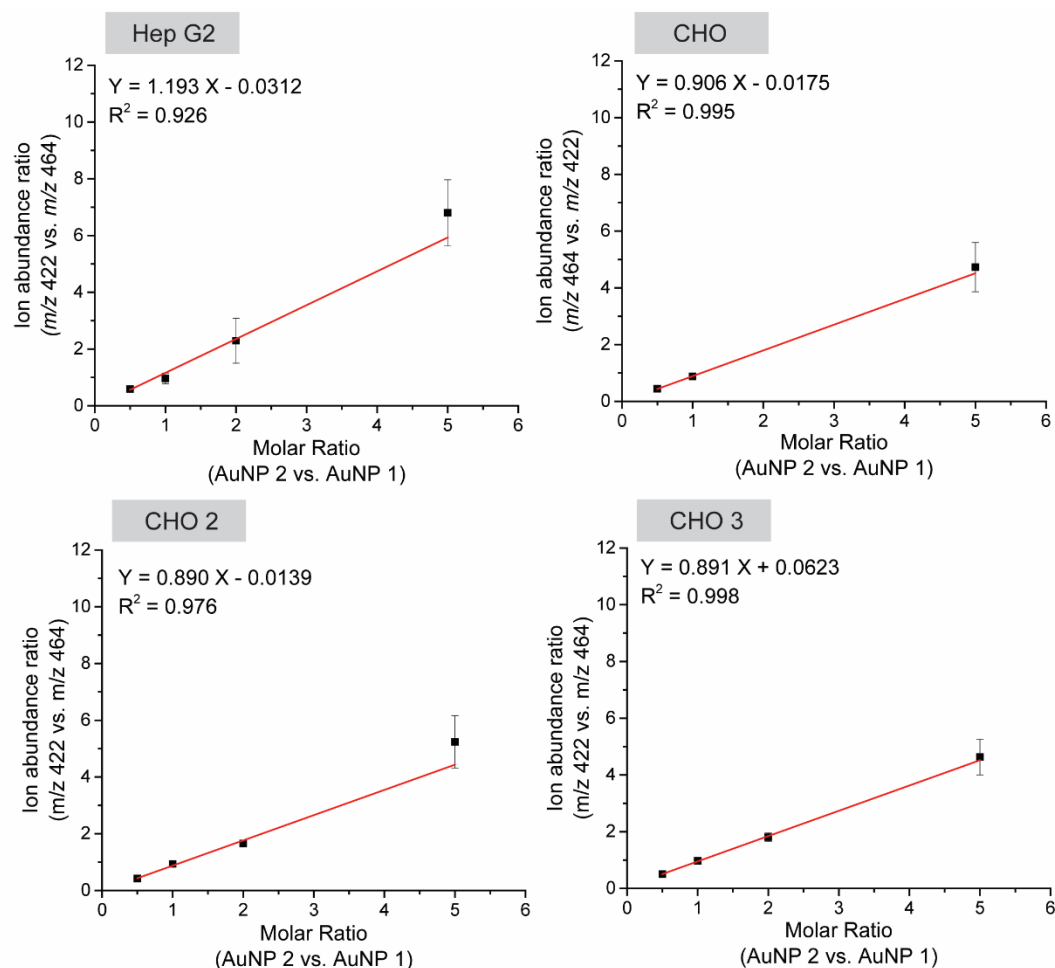
Figure 1.9 LDI-MS calibration curves for AuNP 2 in cell lysate. Increasing concentrations of AuNP 2 were mixed with AuNP 1 (internal standard) and spiked into cell lysate of HeLa, Hep G2, CHO, CHO 2 and CHO 3 cells. After centrifugation, the resulting pellets were deposited on a stainless steel target and analyzed with LDI-MS. Molecular ions of both AuNPs were plotted against molar ratios.

Calculation of absolute quantity of total, internalized and cell surface-bound AuNP 2 by coupling LDI-MS and ICP-MS

After incubation and addition of the internal standard (AuNP 1), the cells are lysed for ICP-MS detection. The gold amount measured from the sample is denoted by X (ng). X arises from contributions from the gold amounts of AuNP 2 (X (AuNP 2) total) and AuNP 1 (X (AuNP 1)). The LDI-MS measured molar ratio between AuNP 2 and AuNP 1 is denoted

12

by Y. Ytotal represents the molar ratio of the total amounts of AuNP 2 to AuNP 1. With equation (1), the absolute amount of total AuNP 2 with cells can be calculated.

Equation (2) describes the absolute amount of AuNP 2 on the cell surface. Ysurface represents the molar ratio of cell surface-bound AuNP 2 to AuNP 1. By subtracting AuNP 2 on cell surface from total amount of AuNP 2 in equation (3), absolute amount for internalization can be determined.

$$\begin{cases} X\,(AuNP\,2)_{total} = X - X\,(AuNP\,1) \\ \frac{X\,(AuNP\,2)_{total}}{X\,(AuNP\,1)} = Y_{total} \end{cases} \quad\quad (1)$$

$$X(AuNP\,2)_{surface} = \frac{Y_{surface}}{Y_{total}} \times X(AuNP\,2)_{total} \quad\quad (2)$$

$$X(AuNP\,2)_{internalization} = X(AuNP\,2)_{total} - X(AuNP\,2)_{surface} \quad\quad (3)$$

1.6 Reference

1. Duncan, B.; Kim, C.; Rotello, V. M. Gold Nanoparticle Platforms as Drug and Biomacromolecule Delivery Systems. *J. Controlled. Release* **2010**, *148*, 122–127.

2. Tao, A. R.; Habas, S.; Yang, P. Shape Control of Colloidal Metal Nanocrystals. *Small* **2008**, *4*, 310–325.

3. Faraji, A. H.; Wipf, P. Nanoparticles in Cellular Drug Delivery. *Bioorg. Med. Chem.* **2009**, *17*, 2950–2962.

4. Meyer, D. E.; Shin, B. C.; Kong, G. A.; Dewhirst, M. W.; Chilkoti, A. Drug Targeting Using Thermally Responsive Polymers and Local Hyperthermia. *J. Controlled. Release* **2001**, 74, 213–224.

5. Hong, R.; Han, G.; F ernández, J. M.; Kim, B. J.; Forbes, N. S.; Rotello, V. M. Glutathione-Mediated Delivery and Release Using Monolayer Protected Nanoparticle Carriers. *J. Am. Chem. Soc.* **2006**, *128*, 1078–1079.

6. Gao, X.; Cui, Y.; Levenson, R. M.; Chung, L. W. K.; Nie, S. In Vivo Cancer Targeting and Imaging with Semiconductor Quantum Dots. *Nat. Biotechnol.* **2004**, *22*, 969–976.

7. Kircher, M. F.; de la Zerda, A.; Jokerst, J. V; Zavaleta, C. L.; Kempen, P. J.; Mittra, E.; Pitter, K.; Huang, R.; Campos, C.; Habte, F.; *et al.* A Brain Tumor Molecular Imaging Strategy Using a New Triple-Modality MRI-Photoacoustic-Raman Nanoparticle. *Nat. Med.* **2012**, *18*, 829–834.

8. Brannon-Peppas, L.; Blanchette, J. O. Nanoparticle and Targeted Systems for Cancer Therapy. *Adv. Drug Delivery Rev.* **2012**, *64*, 206–212.

9. Verma, A.; Stellacci, F. Effect of Surface Properties on Nanoparticle-Cell Interactions. *Small* **2010**, *6*, 12–21.

10. Lesniak, A.; Salvati, A. Nanoparticle Adhesion to the Cell Membrane and Its Effect on Nanoparticle Uptake Efficiency. *J. Am. Chem. Soc.* **2013**, *135*, 1438–1444.

11. Verma, A.; Uzun, O.; Hu, Y.; Hu, Y.; Han, H.-S.; Watson, N.; Chen, S.; Irvine, D. J.; Stellacci, F. Surface-Structure-Regulated Cell-Membrane Penetration by Monolayer-Protected Nanoparticles. *Nat. Mater.* **2008**, *7*, 588–595.

12. Sokolov, K.; Follen, M.; Aaron, J.; Pavlova, I.; Malpica, A.; Lotan, R.; Richards-kortum, R. Advances in Brief Real-Time Vital Optical Imaging of Precancer Using Anti-Epidermal Growth Factor Receptor Antibodies Conjugated to Gold Nanoparticles 1. *Cancer Res.* **2004**, *63*, 1999–2004.

13. Boal, A.; Ilhan, F.; DeRouchey, J.; Thurn-Albrecht, T.; Russell, T.; Rotello, V. Self-Assembly of Nanoparticles into Structured Spherical and Network Aggregates. *Nature* **2000**, *404*, 746–748.

14. Genovese, D.; Bonacchi, S.; Juris, R.; Montalti, M.; Prodi, L.; Rampazzo, E.; Zaccheroni, N. Prevention of Self-Quenching in Fluorescent Silica Nanoparticles by Efficient Energy Transfer. *Angew. Chem., Int. Ed.* **2013**, *52*, 5965–5968.

15. Chithrani, B. D.; Ghazani, A. a; Chan, W. C. W. Determining the Size and Shape Dependence of Gold Nanoparticle Uptake into Mammalian Cells. *Nano Lett.* **2006**, *6*, 662–668.

16. Kim, J. A.; Åberg, C.; Salvati, A.; Dawson, K. A. Role of Cell Cycle on the Cellular Uptake and Dilution of Nanoparticles in a Cell Population. *Nat. Nanotechnol.* **2011**, *7*, 62–68.

17. Cho, E. C.; Xie, J.; Wurm, P. a; Xia, Y. Understanding the Role of Surface Charges in Cellular Adsorption versus Internalization by Selectively Removing Gold Nanoparticles on the Cell Surface with a I2/KI Etchant. *Nano Lett.* **2009**, *9*, 1080–1084.

18. Braun, G. B.; Friman, T.; Pang, H.-B.; Pallaoro, A.; Hurtado de Mendoza, T.; Willmore, A.-M. a; Kotamraju, V. R.; Mann, A. P.; She, Z.-G.; Sugahara, K. N.; *et al.* Etchable Plasmonic Nanoparticle Probes to Image and Quantify Cellular Internalization. *Nat. Mater.* **2014**, *13*, 904–911.

19. Cooper, R. A. Iodine Revisited. *Int. Wound J.* **2007**, *4*, 124-137

20．Zhu, Z.-J.; Rotello, V. M.; Vachet, R. W. Engineered Nanoparticle Surfaces for Improved Mass Spectrometric Analyses. *Analyst* **2009**, *134*, 2183–2188.

21. Yan, B.; Zhu, Z.-J.; Miranda, O. R.; Chompoosor, A.; Rotello, V. M.; Vachet, R. W. Laser Desorption/ionization Mass Spectrometry Analysis of Monolayer-Protected Gold Nanoparticles. *Anal. Bioanal. Chem.* **2010**, *396*, 1025–1035.

22. Yan, B.; Jeong, Y.; Mercante, L. a; Tonga, G. Y.; Kim, C.; Zhu, Z.-J.; Vachet, R. W.; Rotello, V. M. Characterization of Surface Ligands on Functionalized Magnetic Nanoparticles Using Laser Desorption/ionization Mass Spectrometry (LDI-MS). *Nanoscale* **2013**, *5*, 5063–5066.

23. Zhu, Z.-J.; Ghosh, P. S.; Miranda, O. R.; Vachet, R. W.; Rotello, V. M. Multiplexed Screening of Cellular Uptake of Gold Nanoparticles Using Laser Desorption/ionization Mass Spectrometry. *J. Am. Chem. Soc.* **2008**, *130*, 14139–14143.

24. Zhu, Z.-J.; Yeh, Y.-C.; Tang, R.; Yan, B.; Tamayo, J.; Vachet, R. W.; Rotello, V. M. Stability of Quantum Dots in Live Cells. *Nat. Chem.* **2011**, *3*, 963–968.

25. Zhu, Z.-J.; Tang, R.; Yeh, Y.-C.; Miranda, O. R.; Rotello, V. M.; Vachet, R. W. Determination of the Intracellular Stability of Gold Nanoparticle Monolayers Using Mass Spectrometry. *Anal. Chem.* **2012**, *84*, 4321–4326.

26. Kim, C. S.; Le, N. D. B.; Xing, Y.; Yan, B.; Tonga, G. Y.; Kim, C.; Vachet, R. W.; Rotello, V. M. The Role of Surface Functionality in Nanoparticle Exocytosis. *Adv. Healthcare Mater.* **2014**, *3*, 1200–1202.

27. Payne, C. K.; Jones, S. A.; Chen, C.; Zhuang, X. Internalization and Trafficking of Cell Surface Proteoglycans and Proteoglycan-Binding Ligands. *Traffic* **2007**, *8*, 389–401.

28. Castellana, E. T.; Russell, D. H. Tailoring Nanoparticle Surface Chemistry to Enhance Laser Desorption Ionization of Peptides and Proteins. *Nano Lett.* **2007**, *7*, 3023–3025.

29 . Wen, X.; Dagan, S.; Wysocki, V. H. Small-Molecule Analysis with Silicon-Nanoparticle-Assisted Laser Desorption/ionization Mass Spectrometry. *Anal. Chem.* **2007**, *79*, 434–444.

30. Chen, C.; Chen, Y. Fe3O4 / TiO2 Core / Shell Nanoparticles as Affinity Probes for the Analysis of Phosphopeptides Using TiO2 Surface-Assisted Laser Desorption / Ionization Mass Spectrometry. *Anal. Chem.* **2005**, *77*, 5912–5919.

31. Chen, S.; Xiong, C.; Liu, H.; Wan, Q.; Hou, J.; He, Q.; Badu-Tawiah, A.; Nie, Z. Mass Spectrometry Imaging Reveals the Sub-Organ Distribution of Carbon Nanomaterials. *Nat. Nanotechnol.* **2015**, *10*, 176–182.

32. Brust, M.; Walker, M.; Bethell, D.; Schiffrin, D. J.; Whyman, R. Synthesis of Thiol-Derivatized Gold Nanoparticles in a Two-Phase Liquid-Liquid System. J. Chem. Soc. Chem. Commun. 1994, 7, 801–802.

33. Templeton, A. C.; Wuelfing, W. P.; Murray, R. W. Monolayer-Protected Cluster Molecules. Acc. Chem. Res. 2000, 33, 27–36.

34. You, C.-C.; Miranda, O. R.; Gider, B.; Ghosh, P. S.; Kim, I.-B.; Erdogan, B.; Krovi, S. A.; Bunz, U. H. F.; Rotello, V. M. Detection and Identification of Proteins Using Nanoparticle-Fluorescent Polymer "Chemical Nose" Sensors. Nat. Nanotechnol. 2007, 2, 318–323.

CHAPTER 2

NANOPARTICLE PROBES FOR QUANTIFYING BIOSURFACE AFFINITY

2.1 Introduction

Understanding and engineering the interactions of synthetic and biomolecular systems with biosurfaces is an important issue in health and personal care. Adhesion to skin is a key feature for drug delivery systems, [1,2,3,4,5,6] wound healing, [7,8] and cosmetics. [9,10,11,12,13] Likewise, adhesion of molecular systems to hair is key to their unique properties in hearing and mechanical systems such as gecko feet, [14] and is essential in the hair care field. [15] In all of these systems, controlled of supramolecular interactions are required to tune both the strength and reversibility of adhesion.

Unravelling the complex interrelationship between size, shape, charge, and structure of materials at biosurfaces is a challenging task. The supramolecularly competitive aqueous environment in which these surfaces function makes multivalent interactions a prerequisite. For this reason, polymers have been used as platforms to study adhesion to hair and skin. [16,17] For example, it has been found that Polyquaternium-24 polymer adsorbs more strongly to skin membranes than Polyquaternium-10 or chitosan. [18] However, polymers are inherently flexible with accessible backbone functionality, making direct assessment of specific interactions difficult. On the other hand, monolayer-protected nanoparticles provide an excellent scaffold to study supramolecular interactions.

Through proper engineering of monolayer structure, nanoparticle systems provide a non-interactive "tabula rasa" that can be decorated with specific chemical functionalities. [19] These particles have been used to quantitatively probe the multivalent interactions of "simple" chemical motifs such as carboxylates and ammonium ions with proteins, [20] nucleic acids, [21] and cells. [22]

In this chapter I report the use of these gold nanoparticles (AuNPs) as scaffolds to probe role of specific supramolecular interactions on adhesion to hair, a model biosurface. These AuNP probes combine their inherent multivalent presentation of functionality with the ability to directly quantify their amount using inductively-coupled plasma mass

spectrometry (ICP-MS). Through this strategy we determined that electrostatics were the strongest driver of adhesion, with cationic particles binding much more strongly than their anionic or neutral counterparts. Surprisingly, it was found that electron-rich aromatic moieties strongly enhanced adhesion, suggesting that cation-π interactions are a potential tool for controlling adhesion.
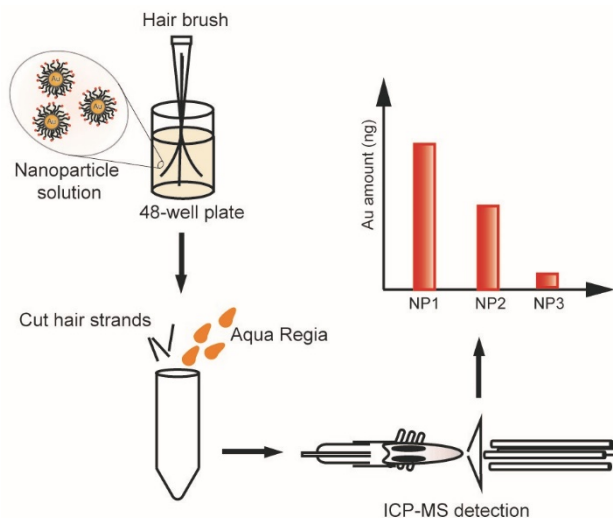
Figure 2.1 Detection of AuNP adsorption on human hair surface using inductively-coupled plasma mass spectrometry (ICP-MS). Three hair strands were immobilized on pipette tips and incubated in different nanoparticle (NP) solutions. Incubated hair strands were cut and digested with Aqua Regia before ICP-MS analysis.

2.2 Result and discussion

AuNPs used in this study featured 2 nm core size and were stabilized by surface monolayers with three functional sections. From the interior to the surface of AuNP, these are alkane thiol, tetra-ethylene glycol and terminal functional groups. These functional sections serve to stabilize AuNP from disassembly, to prevent irreversible interaction between AuNPs and biological surfaces, and to interact with the surrounding environment respectively. When these structural parameters remain unchanged, terminal groups can be varied to explore the effect of chemical functionality with a structurally unified and stable scaffold.[21]
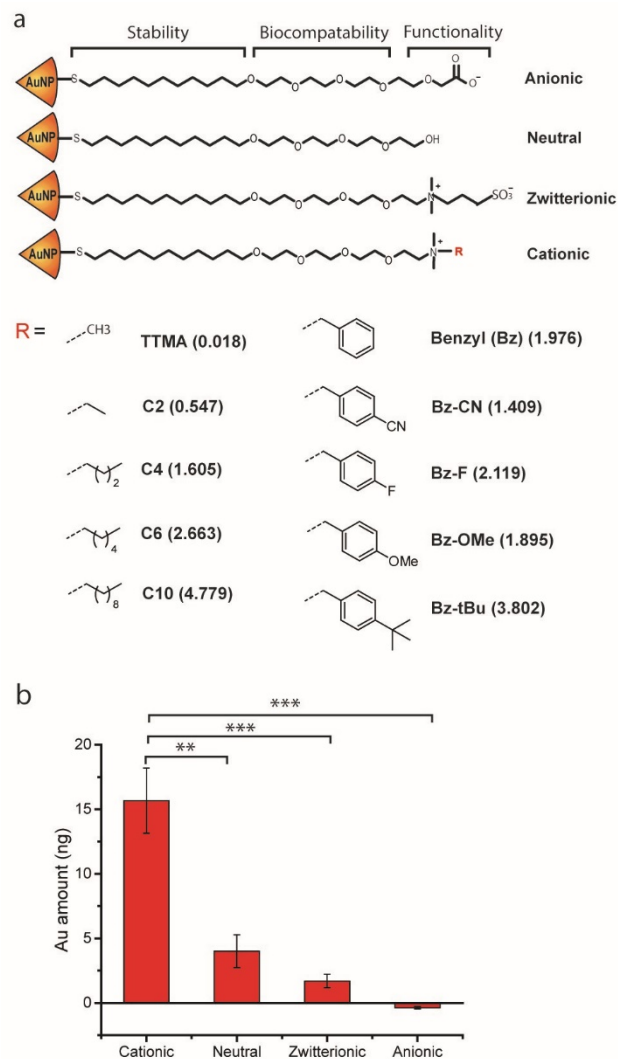
Figure 2.2 (a) Structures of gold nanoparticles (AuNPs) used in this study, the calculated log P of the terminal groups are shown in brackets. (b) The effect of charge on hair adsorption, cationic NP shows the highest adsorption on hair surface compared to neutral, zwiterionic and anionic NPs.

In our initial study, we investigated the effect of NP charge types including cationic, neutral, zwitterionic and anionic AuNPs (Figure 2a). Hair is composed mainly of keratin and has an isoelectric point of 3.7.[23] The keratin fibres on hair surface are covalently coated with 18-methyl eicosanoic acid.[24] This lipid layer provides protection and concomitant hydrophobic hair surface. To determine the adsorption level of AuNPs on hair after incubation, the gold amount adsorbed on hair was measured by ICP-MS (Figure 1). Comparing to other charge types of

AuNPs, cationic AuNPs adsorbed much more efficiently to the hair (Figure 2b). This observation is consistent with other study where hair has strong interaction with cationic polymers used as conditioning agents.[25] Also, the hair surface was found to have high adhesion force to amine decorated tips in AFM.[26] Due to the negatively charged hair surface, cationic AuNPs can bind strongly to hair via electrostatic interaction. These ionic bonds in addition to the multivalence of the particles are strong enough to hold the particles on the hair surface even when it is being rinsed off extensively. Since positive charge is necessary for hair adsorption, we took a further step in designing a library of cationic AuNPs by modifying the terminal R groups on cationic ligand of AuNP to understand the effect of chemical functionality on hair adsorption (Figure 2a).

As mentioned before, hair surface is expected to be hydrophobic. Thus, we hypothesized that terminal groups with higher hydrophobicity should exhibit enhanced adsorption. To test the hypothesis, R group on cationic AuNPs was modified to present a variety of chemical functionalities with an increased in hydrophobicity represented by calcuated log P (See bracketed numbers in Figure 2a). When Au amount in hair was plotted against log P of terminal groups, we surprisingly found that hydrophobicity did not determine AuNP absorption level, indicated by the scattered sample points and a very poor R-squared value (Figure 3a). A clear trend was shown only when the hydrophobicity of the AuNP was varied by the length of the alkyl chain (TTMA, C2, C4, C6, C10) (Figure 3b).

However, the hair adsorption trend of the increased alkyl chain on the AuNP was not in agreement with our hypothesis, in which the higher the hydrophobicity of the AuNP, the lower the adsorption of the particles on hair. The reason for this observation is probably due to steric effect provided by longer alkyl chain.[27] This phenomenon was demonstrated in previous study. Hydrogen-deuterium exchange of the amine groups was hindered if they were buried deeper along the alkyl ligand on AuNPs.[28] In our case, alkyl chains shield the electrostatic interaction between quaternary amonium on AuNPs and negatively charged hair surface. Therefore, the overall decrease of hair adsorption as the hydrophobicity of the R groups increases

can be explained by the blockage of electrostatic interaction, which was not fully compensated by increased hydrophobic effect.
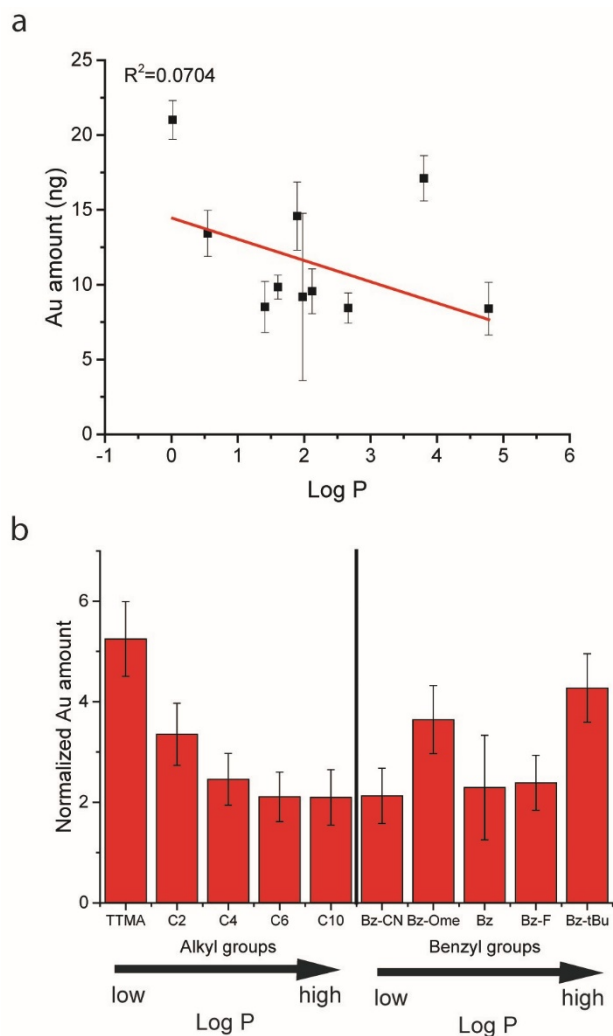
Figure 2.3 Screening of cationic AuNPs library. (a) Hydrophobicity of terminal groups does not determine the level of adsorption. (b) Effect of hydrophobicity determined by alkyl chains and aromatic rings. The AuNP adsorption was normalized to that of TEGOH AuNP.

An interesting and unexpected discovery was found with aromatic terminated AuNPs. Unlike alkyl functional groups, the adsorption of aromatic AuNPs is largely dependent on substitutes on aromatic ring rather than hydrophobic variation. Particles with electron donating substitutes such as methoxyl and tert-butyl groups show a significant enhancement of adsorption compared to particles with no

substitute or electron withdrawing groups (Figure 3b). This interesting finding might be due to cation-π interaction. The exposed charged residues on α-helical keratin fibers carry net negative charge; however, there are discernible positively-charged domains rich in lysine and arginine.[29] These domains can provide interacting sites for electron rich aromatic ring via cation-π interaction.[30] Therefore, the adsorption prompted by electron donating substitutes on AuNPs suggests similar interaction occurs in the nanoparticle keratin fiber interface.
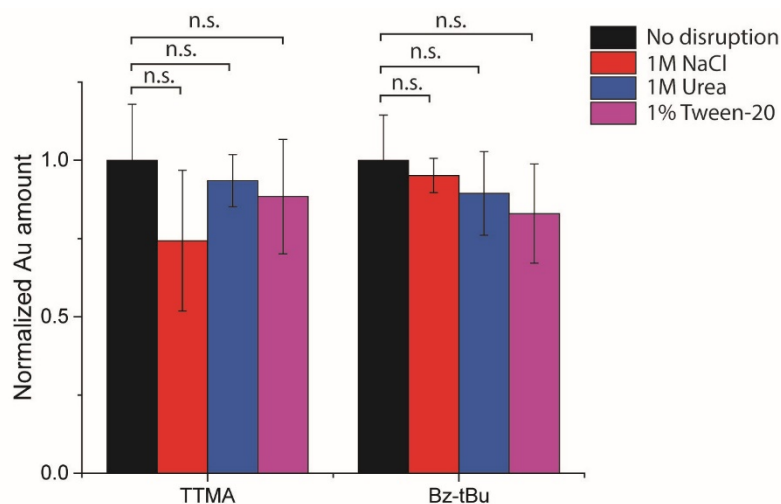
Figure 2.4 Disruption of interaction between AuNPs and hair surfaces with 1 M NaCl, 1 M urea and 1 % Tween-20 (w/v %). The binding of AuNPs after disruption is normalized to that of no disruption of corresponding AuNPs.

Since the working environments for hair adhesive materials usually are not in deionized water. To demonstrate that our findings can also be applicable in complex mixture, we tried the interaction with the presence of three representative disrupting agents, sodium chloride, urea and tween-20. Two nanoparticles, TTMA and Bz-tBu with high adsorption level but different driving forces were chosen. Under these three conditions, no significant decrease of gold adsorption was observed, showing that the interactions between selected AuNPs and hair surface were not disrupted by any of these interfering agents (Figure 4). This strong interaction demonstrates a favourable binding due to the multivalency of AuNPs to

a large and rigid hair surface. This could be the reason why even when entropy is unfavourable upon their binding, the selected AuNPs can still enhance the binding affinity to the biological substrates, which is not seen in typical small molecules.

2.3 Experimental section

Synthesis and characterization of AuNPs. The Brust-Schiffrin two-phase synthesis method was used for synthesis of AuNPs with core diameters around 2 nm. [31] After that, the Murray place-exchange method was used to obtain functionalized AuNPs. [32] The octanol-water partition coefficients (LogP) of the terminal groups of AuNP surface ligands were calculated using ChemDraw Ultra 8.0.

Interaction between hair and AuNPs. Three individual strands of non-treated human hair were immobilized in 10 μL pipet tips with hot glue, 0.6 cm of each hair strand was exposed from the pipette tip to make miniature "hair brushes". The hair brushes were then assembled in a pipette tip rack to form an array of hair brushes. Then the hair brush array was placed upon 48-well plates to interact with 300 uL 100 nM AuNPs solution for 5 minutes at room temperature. The incubation was followed by 3 cycles of rinsing in 300 uL deionized water, 2 minutes for each cycle.

ICP-MS measurement and sample preparation. After incubation, the exposed hair strands were cut and collected in 15 mL conical tubes. Samples were furthered digested by 1mL of aqua regia (70%/30% HCl/HNO3) (highly corrosive, operate with cautions). After 2 hours of digestion, the samples were diluted to 4mL with deionized water. A series of gold standard solutions (20, 10, 5, 2, 1, 0.5, 0.2, 0 ppb) was prepared for each experiment, and these standard solutions also contained 1 mL of aqua regia. The ICP-MS analyses were performed on a Perkin-Elmer NexION 300X ICP-MS. 197 Au was measured under standard mode. Nebulizer flow rate: 0.91-1 L/min; rf power: 1600 W; plasma Ar flow rate: 18 L/min; dwelling time: 50 ms.

2.4 Conclusion

In summary, we have used surface engineered AuNPs to understand the chemical functionalities contributed to adsorption on human hair. Human hair

surface was known to be negatively charged and hydrophobic due to the presence of sulfonate and 18-MEA. Our findings suggests that even though cation is necessary, there are no correlation between nanoparticle hydrophobicity and adsorption. Other factors including structural hindrance and cation-pi interaction are new aspects to be considered when designing new adhesive nanomaterials to hair surface. Our findings are not only applicable in water but also with the presence of chaotropic reagents. The strategy to use AuNPs scaffold coupled with sensitive ICP-MS detection is beneficial in eliminating biological noise, enabling application to a variety of biological surfaces in future studies.

2.5 Reference

1. Prow, T. W.; Grice, J. E.; Lin, L. L.; Faye, R.; Butler, M.; Becker, W.; Wurm, E. M. T.; Yoong, C.; Robertson, T. a; Soyer, H. P.; *et al.* Nanoparticles and Microparticles for Skin Drug Delivery. *Adv. Drug Delivery Rev.* **2011**, *63*, 470–491. 491.

2. Arangoa, M. A.; Ponchel, G.; Orecchioni, A. M.; Renedo, M. J.; Duchêne, D.; Irache, J. M. Bioadhesive Potential of Gliadin Nanoparticulate Systems. *Eur. J. Pharm. Sci.* **2000**, *11*, 333–341.

3. Reineke, J.; Cho, D. Y.; Dingle, Y. L.; Cheifetz, P.; Laulicht, B.; Lavin, D.; Furtado, S.; Mathiowitz, E. Can Bioadhesive Nanoparticles Allow for More Effective Particle Uptake from the Small Intestine? *J. Controlled Release* **2013**, *170*, 477–484.

4. Salman, H. H.; Gamazo, C.; de Smidt, P. C.; Russell-Jones, G.; Irache, J. M. Evaluation of Bioadhesive Capacity and Immunoadjuvant Properties of Vitamin B(12)-Gantrez Nanoparticles. *Pharm. Res.* **2008**, *25*, 2859–2868.

5. Porfire, A. S.; Zabaleta, V.; Gamazo, C.; Leucuta, S. E.; Irache, J. M. Influence of Dextran on the Bioadhesive Properties of Poly (anhydride) Nanoparticles. *Int. J. Pharm.* **2010**, *390*, 37–44.

6. Melgar-Lesmes, P.; Morral-Ruíz, G.; Solans, C.; García-Celma, M. J. Quantifying the Bioadhesive Properties of Surface-Modified Polyurethane-Urea Nanoparticles in the Vascular Network. *Colloids Surf., B* **2014**, *118*, 280–288.

7. Meddahi-Pellé, A.; Legrand, A.; Marcellan, A.; Louedec, L.; Letourneur, D.; Leibler, L. Organ Repair, Hemostasis, and in Vivo Bonding of Medical Devices by Aqueous Solutions of Nanoparticles. *Angew. Chem., Int. Ed.* **2014**, *53*, 6369–6373.

8. Shi, J.; Votruba, A. R.; Farokhzad, O. C.; Langer, R. Nanotechnology in Drug Delivery and Tissue Engineering: From Discovery to Applications. *Nano Letters*, **2010**, *10*, 3223–3230.

9. Raj, S.; Sumod, U.; Jose, S.; Sabitha, M. Nanotechnology in Cosmetics: Opportunities and Challenges. *J. Pharm. BioAllied Sci.* **2012**, *4*, 186.

10. Üner, M.; Wissing, S. A.; Yener, G.; Müller, R. H. Skin Moisturizing Effect and Skin Penetration of Ascorbyl Palmitate Entrapped in Solid Lipid Nanoparticles (SLN) and Nanostructured Lipid Carriers (NLC) Incorporated into Hydrogel. *Pharmazie* **2005**, *60*, 751–755.

11. Müller, R. H.; Radtke, M.; Wissing, S. A. Nanostructured Lipid Matrices for Improved Microencapsulation of Drugs. *Int. J. Pharm.* **2002**, *242*, 121–128.

12. Kasemo, B. Biological Surface Science. *Surf. Sci.* **2002**, *500*, 656–677.

13. Mu, L.; Sprando, R. L. Application of Nanotechnology in Cosmetics. *Pharm. Res.* **2010**, *27*, 1746–1749.

14. (a) P.F.A.Maderson. Keratinized Epidermal Derivatives as an Aid to Climbing in Gekkonid Lizards. *Nature* **1964**, *203*, 780–781. (b) Geim, A. K.; Dubonos, S. V; Grigorieva, I. V; Novoselov, K. S.; Zhukov, A. A.; Shapoval, S. Y. Microfabricated Adhesive Mimicking Gecko Foot-Hair. *Nat. Mater.* **2003**, *2*, 461–463.

15 . LaTorre, C.; Bhushan, B. Nanotribological Effects of Hair Care Products and Environment on Human Hair Using Atomic Force Microscopy. *J. Vac. Sci. Technol., A* **2005**, *23*, 1034–1045.

16. Venkatraman, S.; Gale, R. Skin Adhesives and Skin Adhesion. 1. Transdermal Drug Delivery Systems. *Biomaterials*, 1998, *19*, 1119–1136.

17. Gray, J. Hair Care and Hair Care Products. *Clin. Dermatol.* **2001**, *19*, 227–236.

18. Goddard, E. D.; Harris, W. C. An ESCA Study of the Substantivity of Conditioning Polymers on Hair Substrates. *J. Soc. Cosmet. Chem.* **1987**, *246*, 233–246.

19. Moyano, D. F.; Rotello, V. M. Nano Meets Biology: Structure and Function at the Nanoparticle Interface. *Langmuir* **2011**, *27*, 10376–10385.

20. Jordan, B. J.; Hong, R.; Gider, B.; Hill, J.; Emrick, T.; Rotello, V. M. Stabilization of α-Chymotrypsin at Air/water Interface through Surface Binding to Gold Nanoparticle Scaffolds. *Soft Matter*, **2006**, *2*, 558.

21. McIntosh, C. M.; Esposito, E. A.; Boal, A. K.; Simard, J. M.; Martin, C. T.; Rotello, V. M. Inhibition of DNA Transcription Using Cationic Mixed Monolayer Protected Gold Clusters. *J. Am. Chem. Soc.* **2001**, *123*, 7626–7629.

22. Zhu, Z. J.; Posati, T.; Moyano, D. F.; Tang, R.; Yan, B.; Vachet, R. W.; Rotello, V. M. The Interplay of Monolayer Structure and Serum Protein Interactions on the Cellular Uptake of Gold Nanoparticles. *Small* **2012**, *8*, 2659–2663.

23. Yu, J.; Yu, D. W.; Checkla, D. M.; Freedberg, I. M.; Bertolino, A. P. Human Hair Keratins. *J. Invest. Dermatol.* **1993**, *101*, 56–59.

24. LaTorre, C.; Bhushan, B. Nanotribological Characterization of Human Hair and Skin Using Atomic Force Microscopy. *Ultramicroscopy* **2005**; 105, 155–175.

25. Ungewiss, J.; Vietzke, J. P.; Rapp, C.; Schmidt-Lewerkühne, H.; Wittern, K. P.; Salzer, R. Quantitative Determination of Cationic Modified Polysaccharides on Hair Using LC-MS and LC-MS-MS. *Anal. Bioanal. Chem.* **2005**, *381*, 1401–1407.

26. Korte, M.; Akari, S.; Kühn, H.; Baghdadli, N. Distribution and Localization of Hydrophobic and Ionic Chemical Groups at the Surface of Bleached Human Hair Fibers. *Langmuir* **2014**, *30*, 12124–12129.

27. Shenhar, R.; Rotello, V. M. Nanoparticles: Scaffolds and Building Blocks. *Acc. Chem. Res.* **2003**, *36*, 549–561.

28. Briggs, C.; Norsten, T. B.; Rotello, V. M. Inhibition and Acceleration of Deuterium Exchange in Amide-Functionalized Monolayer-Protected Gold Clusters. *Chem. Commun.* **2002**, 1890–1891.

29. Lee, C.-H.; Kim, M.-S.; Chung, B. M.; Leahy, D. J.; Coulombe, P. a. Structural Basis for Heteromeric Assembly and Perinuclear Organization of Keratin Filaments. *Nat. Struct. Mol. Biol.* **2012**, *19*, 707–715.

30. Crowley, P. B.; Golovin, A. Cation-Pi Interactions in Protein-Protein Interfaces. *Proteins* **2005**, *59*, 231–239.

31. Templeton, A. C.; Wuelfing, W. P.; Murray, R. W. Monolayer-Protected Cluster Molecules. *Acc. Chem. Res.* **2000**, *33*, 27–36.

32. You, C.-C.; Miranda, O. R.; Gider, B.; Ghosh, P. S.; Kim, I.-B.; Erdogan, B.; Krovi, S. A.; Bunz, U. H. F.; Rotello, V. M. Detection and Identification of Proteins Using Nanoparticle-Fluorescent Polymer "Chemical Nose" Sensors. *Nat. Nanotechnol.* **2007**, *2*, 318–323.

BIBILOGRAPHY

Arangoa, M. A.; Ponchel, G.; Orecchioni, A. M.; Renedo, M. J.; Duchêne, D.; Irache, J. M. Bioadhesive Potential of Gliadin Nanoparticulate Systems. *Eur. J. Pharm. Sci.* **2000**, *11*, 333–341.

Boal, A.; Ilhan, F.; DeRouchey, J.; Thurn-Albrecht, T.; Russell, T.; Rotello, V. Self-Assembly of Nanoparticles into Structured Spherical and Network Aggregates. *Nature* **2000**, *404*, 746–748.

Brannon-Peppas, L.; Blanchette, J. O. Nanoparticle and Targeted Systems for Cancer Therapy. *Adv. Drug Delivery Rev.* **2012**, *64*, 206–212.

Braun, G. B.; Friman, T.; Pang, H.-B.; Pallaoro, A.; Hurtado de Mendoza, T.; Willmore, A.-M. a; Kotamraju, V. R.; Mann, A. P.; She, Z.-G.; Sugahara, K. N.; *et al.* Etchable Plasmonic Nanoparticle Probes to Image and Quantify Cellular Internalization. *Nat. Mater.* **2014**, *13*, 904–911.

Briggs, C.; Norsten, T. B.; Rotello, V. M. Inhibition and Acceleration of Deuterium Exchange in Amide-Functionalized Monolayer-Protected Gold Clusters. *Chem. Commun.* **2002**, 1890–1891.

Brust, M.; Walker, M.; Bethell, D.; Schiffrin, D. J.; Whyman, R. Synthesis of Thiol-Derivatized Gold Nanoparticles in a Two-Phase Liquid-Liquid System. J. Chem. Soc. Chem. Commun. 1994, 7, 801–802.

Castellana, E. T.; Russell, D. H. Tailoring Nanoparticle Surface Chemistry to Enhance Laser Desorption Ionization of Peptides and Proteins. *Nano Lett.* **2007**, *7*, 3023–3025.

Chen, C.; Chen, Y. Fe3O4 / TiO2 Core / Shell Nanoparticles as Affinity Probes for the Analysis of Phosphopeptides Using TiO2 Surface-Assisted Laser Desorption / Ionization Mass Spectrometry. *Anal. Chem.* **2005**, *77*, 5912–5919.

Chen, S.; Xiong, C.; Liu, H.; Wan, Q.; Hou, J.; He, Q.; Badu-Tawiah, A.; Nie, Z. Mass Spectrometry Imaging Reveals the Sub-Organ Distribution of Carbon Nanomaterials. *Nat. Nanotechnol.* **2015**, *10*, 176–182.

Chithrani, B. D.; Ghazani, A. a; Chan, W. C. W. Determining the Size and Shape Dependence of Gold Nanoparticle Uptake into Mammalian Cells. *Nano Lett.* **2006**, *6*, 662–668.

Cho, E. C.; Xie, J.; Wurm, P. a; Xia, Y. Understanding the Role of Surface Charges in Cellular Adsorption versus Internalization by Selectively Removing Gold Nanoparticles on the Cell Surface with a I2/KI Etchant. *Nano Lett.* **2009**, *9*, 1080–1084.

Cooper, R. A. Iodine Revisited. *Int. Wound J.* **2007**, *4*, 124-137

Crowley, P. B.; Golovin, A. Cation-Pi Interactions in Protein-Protein Interfaces. *Proteins* **2005**, *59*, 231–239.

Duncan, B.; Kim, C.; Rotello, V. M. Gold Nanoparticle Platforms as Drug and Biomacromolecule Delivery Systems. *J. Controlled. Release* **2010**, *148*, 122–127.

Faraji, A. H.; Wipf, P. Nanoparticles in Cellular Drug Delivery. *Bioorg. Med. Chem.* **2009**, *17*, 2950–2962.

Gao, X.; Cui, Y.; Levenson, R. M.; Chung, L. W. K.; Nie, S. In Vivo Cancer Targeting and Imaging with Semiconductor Quantum Dots. *Nat. Biotechnol.* **2004**, *22*, 969–976.

Geim, A. K.; Dubonos, S. V; Grigorieva, I. V; Novoselov, K. S.; Zhukov, A. A.; Shapoval, S. Y. Microfabricated Adhesive Mimicking Gecko Foot-Hair. *Nat. Mater.* **2003**, *2*, 461–463.

Genovese, D.; Bonacchi, S.; Juris, R.; Montalti, M.; Prodi, L.; Rampazzo, E.; Zaccheroni, N. Prevention of Self-Quenching in Fluorescent Silica Nanoparticles by Efficient Energy Transfer. *Angew. Chem., Int. Ed.* **2013**, *52*, 5965–5968.

Goddard, E. D.; Harris, W. C. An ESCA Study of the Substantivity of Conditioning Polymers on Hair Substrates. *J. Soc. Cosmet. Chem.* **1987**, *246*, 233–246.

Gray, J. Hair Care and Hair Care Products. *Clin. Dermatol.* **2001**, *19*, 227–236.

Hong, R.; Han, G.; F ernández, J. M.; Kim, B. J.; Forbes, N. S.; Rotello, V. M. Glutathione-Mediated Delivery and Release Using Monolayer Protected Nanoparticle Carriers. *J. Am. Chem. Soc.* **2006**, *128*, 1078–1079.

Jordan, B. J.; Hong, R.; Gider, B.; Hill, J.; Emrick, T.; Rotello, V. M. Stabilization of α-Chymotrypsin at Air/water Interface through Surface Binding to Gold Nanoparticle Scaffolds. *Soft Matter*, 2006, *2*, 558.

Kasemo, B. Biological Surface Science. *Surf. Sci.* **2002**, *500*, 656–677.

Kim, C. S.; Le, N. D. B.; Xing, Y.; Yan, B.; Tonga, G. Y.; Kim, C.; Vachet, R. W.; Rotello, V. M. The Role of Surface Functionality in Nanoparticle Exocytosis. *Adv. Healthcare Mater.* **2014**, *3*, 1200–1202.

Kim, J. A.; Åberg, C.; Salvati, A.; Dawson, K. A. Role of Cell Cycle on the Cellular Uptake and Dilution of Nanoparticles in a Cell Population. *Nat. Nanotechnol.* **2011**, *7*, 62–68.

Kircher, M. F.; de la Zerda, A.; Jokerst, J. V; Zavaleta, C. L.; Kempen, P. J.; Mittra, E.; Pitter, K.; Huang, R.; Campos, C.; Habte, F.; *et al.* A Brain Tumor Molecular Imaging Strategy Using a New Triple-Modality MRI-Photoacoustic-Raman Nanoparticle. *Nat. Med.* **2012**, *18*, 829–834.

Korte, M.; Akari, S.; Kühn, H.; Baghdadli, N. Distribution and Localization of Hydrophobic and Ionic Chemical Groups at the Surface of Bleached Human Hair Fibers. *Langmuir* **2014**, *30*, 12124–12129.

LaTorre, C.; Bhushan, B. Nanotribological Characterization of Human Hair and Skin Using Atomic Force Microscopy. *Ultramicroscopy* **2005**; 105, 155–175.

LaTorre, C.; Bhushan, B. Nanotribological Effects of Hair Care Products and Environment on Human Hair Using Atomic Force Microscopy. *J. Vac. Sci. Technol., A* **2005**, *23*, 1034–1045.

Lee, C.-H.; Kim, M.-S.; Chung, B. M.; Leahy, D. J.; Coulombe, P. a. Structural Basis for Heteromeric Assembly and Perinuclear Organization of Keratin Filaments. *Nat. Struct. Mol. Biol.* **2012**, *19*, 707–715.

Lesniak, A.; Salvati, A. Nanoparticle Adhesion to the Cell Membrane and Its Effect on Nanoparticle Uptake Efficiency. *J. Am. Chem. Soc.* **2013**, *135*, 1438–1444.

Manderson. P.F.A. Keratinized Epidermal Derivatives as an Aid to Climbing in Gekkonid Lizards. *Nature* **1964**, *203*, 780–781.

McIntosh, C. M.; Esposito, E. A.; Boal, A. K.; Simard, J. M.; Martin, C. T.; Rotello, V. M. Inhibition of DNA Transcription Using Cationic Mixed Monolayer Protected Gold Clusters. *J. Am. Chem. Soc.* **2001**, *123*, 7626–7629.

Meddahi-Pellé, A.; Legrand, A.; Marcellan, A.; Louedec, L.; Letourneur, D.; Leibler, L. Organ Repair, Hemostasis, and in Vivo Bonding of Medical Devices by Aqueous Solutions of Nanoparticles. *Angew. Chem., Int. Ed.* **2014**, *53*, 6369–6373.

Melgar-Lesmes, P.; Morral-Ruíz, G.; Solans, C.; García-Celma, M. J. Quantifying the Bioadhesive Properties of Surface-Modified Polyurethane-Urea Nanoparticles in the Vascular Network. *Colloids Surf., B* **2014**, *118*, 280–288.

Meyer, D. E.; Shin, B. C.; Kong, G. A.; Dewhirst, M. W.; Chilkoti, A. Drug Targeting Using Thermally Responsive Polymers and Local Hyperthermia. *J. Controlled. Release* **2001**, 74, 213–224.

Moyano, D. F.; Rotello, V. M. Nano Meets Biology: Structure and Function at the Nanoparticle Interface. *Langmuir* **2011**, *27*, 10376–10385.

Mu, L.; Sprando, R. L. Application of Nanotechnology in Cosmetics. *Pharm. Res.* **2010**, *27*, 1746–1749.

Müller, R. H.; Radtke, M.; Wissing, S. A. Nanostructured Lipid Matrices for Improved Microencapsulation of Drugs. *Int. J. Pharm.* **2002**, *242*, 121–128.

Payne, C. K.; Jones, S. A.; Chen, C.; Zhuang, X. Internalization and Trafficking of Cell Surface Proteoglycans and Proteoglycan-Binding Ligands. *Traffic* **2007**, *8*, 389–401.

Porfire, A. S.; Zabaleta, V.; Gamazo, C.; Leucuta, S. E.; Irache, J. M. Influence of Dextran on the Bioadhesive Properties of Poly (anhydride) Nanoparticles. *Int. J. Pharm.* **2010**, *390*, 37–44.

Prow, T. W.; Grice, J. E.; Lin, L. L.; Faye, R.; Butler, M.; Becker, W.; Wurm, E. M. T.; Yoong, C.; Robertson, T. a; Soyer, H. P.; *et al.* Nanoparticles and Microparticles for Skin Drug Delivery. *Adv. Drug Delivery Rev.* **2011**, *63*, 470–491. 491.

Raj, S.; Sumod, U.; Jose, S.; Sabitha, M. Nanotechnology in Cosmetics: Opportunities and Challenges. *J. Pharm. BioAllied Sci.* **2012**, *4*, 186.

Reineke, J.; Cho, D. Y.; Dingle, Y. L.; Cheifetz, P.; Laulicht, B.; Lavin, D.; Furtado, S.; Mathiowitz, E. Can Bioadhesive Nanoparticles Allow for More Effective Particle Uptake from the Small Intestine? *J. Controlled Release* **2013**, *170*, 477–484.

Salman, H. H.; Gamazo, C.; de Smidt, P. C.; Russell-Jones, G.; Irache, J. M. Evaluation of Bioadhesive Capacity and Immunoadjuvant Properties of Vitamin B(12)-Gantrez Nanoparticles. *Pharm. Res.* **2008**, *25*, 2859–2868.

Shenhar, R.; Rotello, V. M. Nanoparticles: Scaffolds and Building Blocks. *Acc. Chem. Res.* **2003**, *36*, 549–561.

Shi, J.; Votruba, A. R.; Farokhzad, O. C.; Langer, R. Nanotechnology in Drug Delivery and Tissue Engineering: From Discovery to Applications. *Nano Letters*, 2010, *10*, 3223–3230.

Sokolov, K.; Follen, M.; Aaron, J.; Pavlova, I.; Malpica, A.; Lotan, R.; Richards-kortum, R. Advances in Brief Real-Time Vital Optical Imaging of Precancer Using Anti-Epidermal Growth Factor Receptor Antibodies Conjugated to Gold Nanoparticles 1. *Cancer Res.* **2004**, *63*, 1999–2004.

Tao, A. R.; Habas, S.; Yang, P. Shape Control of Colloidal Metal Nanocrystals. *Small* **2008**, *4*, 310–325.

Templeton, A. C.; Wuelfing, W. P.; Murray, R. W. Monolayer-Protected Cluster Molecules. *Acc. Chem. Res.* **2000**, *33*, 27–36.

Üner, M.; Wissing, S. A.; Yener, G.; Müller, R. H. Skin Moisturizing Effect and Skin Penetration of Ascorbyl Palmitate Entrapped in Solid Lipid Nanoparticles (SLN) and Nanostructured Lipid Carriers (NLC) Incorporated into Hydrogel. *Pharmazie* **2005**, *60*, 751–755.

Ungewiss, J.; Vietzke, J. P.; Rapp, C.; Schmidt-Lewerkühne, H.; Wittern, K. P.; Salzer, R. Quantitative Determination of Cationic Modified Polysaccharides on Hair Using LC-MS and LC-MS-MS. *Anal. Bioanal. Chem.* **2005**, *381*, 1401–1407.

Venkatraman, S.; Gale, R. Skin Adhesives and Skin Adhesion. 1. Transdermal Drug Delivery Systems. *Biomaterials*, 1998, *19*, 1119–1136.

Verma, A.; Stellacci, F. Effect of Surface Properties on Nanoparticle-Cell Interactions. *Small* **2010**, *6*, 12–21.

Verma, A.; Uzun, O.; Hu, Y.; Hu, Y.; Han, H.-S.; Watson, N.; Chen, S.; Irvine, D. J.; Stellacci, F. Surface-Structure-Regulated Cell-Membrane Penetration by Monolayer-Protected Nanoparticles. *Nat. Mater.* **2008**, *7*, 588–595.

Wen, X.; Dagan, S.; Wysocki, V. H. Small-Molecule Analysis with Silicon-Nanoparticle-Assisted Laser Desorption/ionization Mass Spectrometry. *Anal. Chem.* **2007**, *79*, 434–444.

Yan, B.; Jeong, Y.; Mercante, L. a; Tonga, G. Y.; Kim, C.; Zhu, Z.-J.; Vachet, R. W.; Rotello, V. M. Characterization of Surface Ligands on Functionalized Magnetic Nanoparticles Using Laser Desorption/ionization Mass Spectrometry (LDI-MS). *Nanoscale* **2013**, *5*, 5063–5066.

Yan, B.; Zhu, Z.-J.; Miranda, O. R.; Chompoosor, A.; Rotello, V. M.; Vachet, R. W. Laser Desorption/ionization Mass Spectrometry Analysis of Monolayer-Protected Gold Nanoparticles. *Anal. Bioanal. Chem.* **2010**, *396*, 1025–1035.

You, C.-C.; Miranda, O. R.; Gider, B.; Ghosh, P. S.; Kim, I.-B.; Erdogan, B.; Krovi, S. A.; Bunz, U. H. F.; Rotello, V. M. Detection and Identification of Proteins Using Nanoparticle-Fluorescent Polymer "Chemical Nose" Sensors. *Nat. Nanotechnol.* **2007**, *2*, 318–323.

Yu, J.; Yu, D. W.; Checkla, D. M.; Freedberg, I. M.; Bertolino, A. P. Human Hair Keratins. *J. Invest. Dermatol.* **1993**, *101*, 56–59.

Zhu, Z.-J.; Ghosh, P. S.; Miranda, O. R.; Vachet, R. W.; Rotello, V. M. Multiplexed Screening of Cellular Uptake of Gold Nanoparticles Using Laser Desorption/ionization Mass Spectrometry. *J. Am. Chem. Soc.* **2008**, *130*, 14139–14143.

Zhu, Z-J.; Posati, T.; Moyano, D. F.; Tang, R.; Yan, B.; Vachet, R. W.; Rotello, V. M. The Interplay of Monolayer Structure and Serum Protein Interactions on the Cellular Uptake of Gold Nanoparticles. *Small* **2012**, *8*, 2659–2663.

Zhu, Z.-J.; Rotello, V. M.; Vachet, R. W. Engineered Nanoparticle Surfaces for Improved Mass Spectrometric Analyses. *Analyst* **2009**, *134*, 2183–2188.

Zhu, Z.-J.; Tang, R.; Yeh, Y.-C.; Miranda, O. R.; Rotello, V. M.; Vachet, R. W. Determination of the Intracellular Stability of Gold Nanoparticle Monolayers Using Mass Spectrometry. *Anal. Chem.* **2012**, *84*, 4321–4326.

Zhu, Z.-J.; Yeh, Y.-C.; Tang, R.; Yan, B.; Tamayo, J.; Vachet, R. W.; Rotello, V. M. Stability of Quantum Dots in Live Cells. *Nat. Chem.* **2011**, *3*, 963–968.